

Modeling of magnetically enhanced capacitively coupled plasma sources: Two frequency discharges

Yang Yang and Mark J. Kushner^{a)}

Department of Electrical and Computer Engineering, Iowa State University, 104 Marston Hall, Ames, Iowa 50011

(Received 2 March 2007; accepted 23 July 2007; published 14 August 2007)

Magnetically enhanced, capacitively coupled radio frequency plasma sources are finding continued use for etching of materials for microelectronics fabrication at a time when multifrequency sources are also being developed. Magnetically enhanced reactive ion etching (MERIE) sources typically use magnetic fields of tens to hundreds of Gauss parallel to the substrate to either increase the plasma density at a given pressure or to lower the operating pressure. Multifrequency sources are used to separately control the magnitude of the ion and radical fluxes (typically with a high frequency source) and the ion energy distributions (typically with a low frequency) to the substrate. In this article, the properties of a two-frequency MERIE reactor are discussed using results from a computational investigation. As in single frequency sources, the reduction in transverse electron mobility as the magnetic field increases can produce a reversal of the electric field in the sheath and an increase in voltage drop across the bulk plasma. These trends decrease ion energies and increase the angular spread of ions. Similar trends are found here, including a field reversal in the sheath at the high frequency electrode. These effects produce a coupling between the high and low frequency sources that compromise the independence of ion production and ion acceleration by the two sources. © 2007 American Vacuum Society. [DOI: 10.1116/1.2771558]

I. INTRODUCTION

Parallel plate capacitively coupled plasma (CCP) sources are widely used for dry etching and deposition of materials for microelectronics fabrication. One method of improving the performance of CCP sources is applying a transverse static magnetic field approximately parallel to the electrodes with the goal of increasing the plasma density for a given pressure. In this configuration the devices are often called magnetically enhanced reactive ion etching (MERIE) reactors.¹⁻⁴ Meanwhile, multifrequency CCP sources have also been developed with the goal of separately controlling ion and radical fluxes and ion energy distributions to the substrate.⁵⁻¹¹ Typically in a two-frequency CCP reactor, power is applied at a lower radio frequency (rf) [a few megahertz (MHz) to 10 MHz] to the lower electrode holding the wafer; and higher frequency power is applied to the upper electrode (tens of MHz to hundreds of MHz). Power at the lower frequency is intended to control the shape of the ion energy distributions to the wafer. Power at the higher frequency is intended to control the production of ions and radicals. (In some variants, both frequencies are applied to the lower electrode.^{12,13}) Thus, it is natural to consider what the unique characteristics are when a reactor combines magnetic enhancement, such as in a MERIE, with multifrequency excitation.

Recently two-frequency CCP sources have been the topic of several investigations. Hebner *et al.*⁵ performed diagnostics of two-frequency CCP reactors operating in argon for frequencies between 10 and 190 MHz. They found that at 50

mTorr, as the 13.56 MHz substrate power was increased from 0 to 1500 W, the electron density was independent of the low frequency (LF) power and only depended on the high frequency (HF) source power (60 MHz). Georgieva *et al.*⁶ computationally investigated Ar/CF₄/N₂ discharges sustained in two-frequency CCP reactors using a one-dimensional particle-in-cell/Monte Carlo model. They found that the average ion bombardment energy increased with both HF and LF voltage amplitudes when the other voltage amplitude is kept constant. The explanation is that the maximum sheath potential increases with the sum of the applied HF and LF voltages. They also observed that when there is only a moderate separation between the LF and HF sources (such as 2 and 27 MHz or 2 and 40 MHz) both voltage sources influenced the plasma characteristics. Upon increasing the HF to 60 and 100 MHz, the plasma density and ion current density show little dependence on the LF source. This trend was also experimentally observed by Kitajima *et al.*⁷ using optical emission spectroscopy in Ar/CF₄ discharges. With the LF kept at 700 kHz, the coupling with the HF source became smaller as the HF increased from 13.56 to 100 MHz.

Goto *et al.*¹⁴ performed diagnostics of two-frequency MERIE reactors operating in argon and H₂. The magnetic field was 500 G below the upper electrode and 50 G above the wafer; and the pressure was 7 mTorr. While the 100 MHz HF power was held constant at 100 W, either increasing the LF power or decreasing the LF frequency decreased the dc bias (became more negative). They concluded that by treating the value of the LF excitation as a process parameter, the ion bombardment energy to the substrate can be effectively controlled without affecting the plasma density.

^{a)}Author to whom correspondence should be addressed; electronic mail: mjk@iastate.edu

Rauf¹⁵ computationally investigated the influence of a radial magnetic field on the interaction of two rf sources in an Ar/C₂F₆ capacitively coupled plasma discharge using a two-dimensional continuum model. He found that for constant voltage the amplitudes of rf currents at the electrodes increased with magnetic field strength over the range of 0–50 G and with source frequency over the range of 13.56–70 MHz. His results indicated that magnetic fields in the range of 0–50 G tend to make the system less nonlinear and to separate the contributions of the rf sources.

In this article, results of a computational investigation of a two-frequency MERIE reactor with plasmas sustained in argon are presented. Systematic trends for ion flux, plasma potential and ion energy, and angular distribution are discussed for a reactor resembling an industrial design. Similar to the trends in a single frequency MERIE,^{16,17} the spatial distribution of the plasma transitioned from edge high to center high with increasing magnetic field. Also, the reduction in the transverse electron mobility as the magnetic field increases can increase the voltage drop across the bulk plasma and produce reversals of the electric fields in both the high and low frequency sheaths. As such, the ion flux impinging the substrate decreases in energy and broadens in angle as the magnetic field increases. The net effect of these trends is at high magnetic fields, while keeping power of the LF and HF sources constant, the coupling between the two plasma sources increases thereby hindering the ability to separately control ion and radical fluxes, and ion energy.

The model used in this study is discussed in Sec. II. Parametric results from our investigation of properties of argon plasmas sustained in a two-frequency MERIE are presented in Sec. III. Concluding remarks are in Sec. IV.

II. DESCRIPTION OF THE MODEL AND REACTION MECHANISM

The model used in this investigation is a two-dimensional fluid hydrodynamics simulation which uses a Monte Carlo simulation (MCS) for secondary electrons emitted from electrodes. The model is described in detail in Ref. 15. Briefly, continuity, momentum, and energy equations for neutrals and ions; continuity and energy equations for electrons and Poisson's equation for the electric potential are integrated in time to obtain a periodic steady state. The resulting electric fields and ion fluxes to surfaces are periodically transferred to the MCS where the transport of secondary electrons emitted from surfaces is addressed. Electron impact source functions and sources of secondary electron current obtained from the MCS are returned to the fluid model. The process is iterated to convergence. Following the last iteration, the converged electric fields and source functions for ions and neutrals are recorded as a function of position and phase in the rf cycle. With these values, the energy and angular distributions of ions and neutrals incident on the substrate are obtained using a heavy particle MCS module and this module is also described in detail in Ref. 16.

Although surface wave and finite wavelength effects can be important as frequencies approach or exceed 100

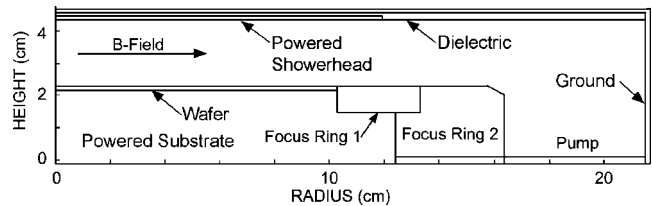


Fig. 1. Geometry for the two-frequency MERIE reactor. The wafer sits on a substrate powered at low frequency surrounded by dielectric focus rings. The showerhead is powered at high frequency and is also surrounded by dielectric. The radial magnetic field is applied parallel to the electrodes.

MHz,^{18,19} or with substrate sizes greater than 20 cm, we have not addressed those effects in this work. All potentials are obtained by solving Poisson's equation assuming an electrostatic approximation. Since our frequencies are at most 40 MHz, the substrate is 20 cm, and the majority of the effects we discuss are most sensitive to transport perpendicular to the electrodes (as opposed to parallel to the electrodes, the direction most affected to finite-wavelength effects); we do not anticipate our results are terribly sensitive to surface wave and finite wavelength effects. Their inclusion would be most evident in the radial distribution of plasma properties.

Powers are separately specified for the LF and HF electrodes and the applied voltages are adjusted to deliver those powers. The powers are computed from $P = (1/\Delta t) \int V I dt$, where V and I are the voltage and total current at the surface of the electrode and Δt is the rf period.

The purpose of this investigation is to study the fundamentals of MERIE reactors using multiple frequencies as opposed to investigating a particular plasma chemical system. As such, the investigation was conducted using only argon as the feedstock gas and whose reaction mechanism is discussed in Ref. 20. The species included in the model are Ar(3s), Ar(4s), Ar(4p), Ar⁺, and electrons. The Ar(4s) is an effective state having a finite lifetime to account for the partial trapping of resonant levels in that manifold. We acknowledge that the details of our observations and conclusions may change using a more complex reaction mechanism, such as the Ar/c-C₄F₈/O₂ mixture previously investigated.¹⁷

III. PLASMA PROPERTIES OF TWO-FREQUENCY MERIE REACTORS

The model reactor used in this study, shown schematically in Fig. 1, is patterned after plasma sources that are commercially available. The base case uses a metal substrate powered at the LF through a blocking capacitor. A conductive Si wafer ($\sigma = 0.01/\Omega \text{ cm}$), 20 cm in diameter, sits in electrical contact with the substrate which is surrounded by a Si ring (focus ring 1, $\epsilon/\epsilon_0 = 12.5$, $\sigma = 10^{-6}/\Omega \text{ cm}$) and dielectric focus ring (focus ring 2, $\epsilon/\epsilon_0 = 8.0$, $\sigma = 10^{-6}/\Omega \text{ cm}$). Gas is injected through a shower head 24 cm in diameter that is powered at the HF. The HF electrode is surrounded by a dielectric having $\epsilon/\epsilon_0 = 8.0$. All other surfaces in the reactor are grounded metal including the annular pump port. A purely radial magnetic field parallel to the wafer will have magnitudes from 0 to 200 G. The approximations that go

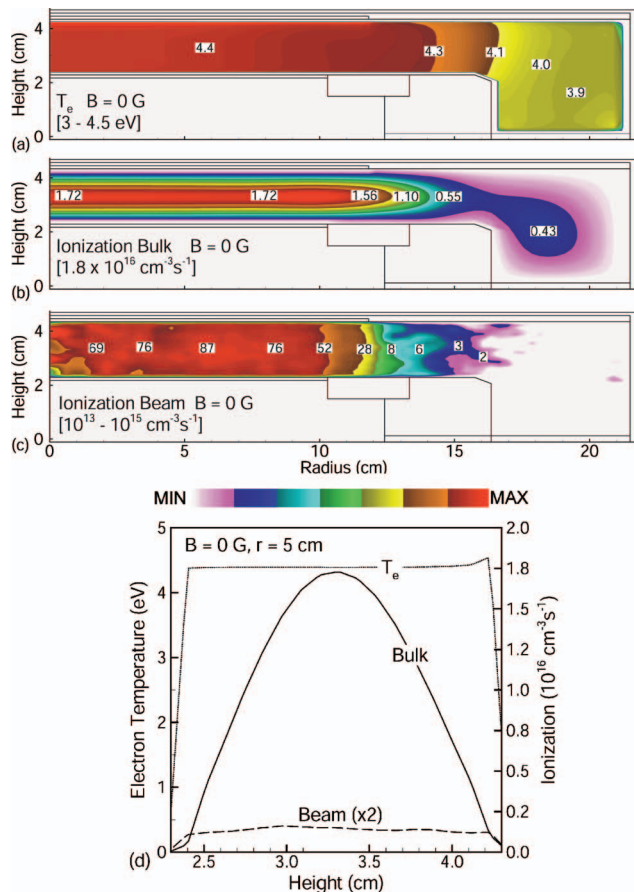


FIG. 2. Plasma properties in the absence of a magnetic field for the base case (Ar, 40 mTorr, $P_{LF}=P_{HF}=500$ W, $\nu_{LF}=5$ MHz, $\nu_{HF}=40$ MHz) without a magnetic field. (a) Electron temperature, (b) ionization by bulk electrons, (c) ionization by beam electrons, and (d) axial values of these quantities at a radius of 5 cm. The maximum value or range of values in each frame is noted. The beam ionization is a log scale over 2 decades with contour labels in units of 10^{13} $\text{cm}^{-3} \text{s}^{-1}$.

with this form of the magnetic field are discussed in Ref. 16. The base case operating conditions are 40 mTorr of argon with a flow rate of 300 sccm, a LF of 5 MHz delivering a power of $P_{LF}=500$ W, and a HF of 40 MHz delivering a power of $P_{HF}=500$ W.

A. Plasma properties with a magnetic field

The electron temperature (T_e), ionization by bulk electrons (S_b) and ionization by beam electrons (S_{eb}) are shown in Fig. 2 without a magnetic field for LF=5 MHz (500 W, 193 V) and HF=40 MHz (500 W, 128 V). These quantities have been averaged over the longer LF cycle. The dc bias on the LF side is -22 V. The Ar^+ density is shown in Fig. 3. For equal powers at LF and HF, the voltage at the high frequency electrode is lower as a consequence of the more efficient power dissipation by electrons at the higher frequency. With an electron density of nearly 10^{11} cm^{-3} , the thermal conductivity is sufficiently high that T_e is nearly uniform across the plasma between the electrodes with a value of 4.4 eV, with there being a small increase at the HF electrode where heating is more efficient. With T_e nearly uniform

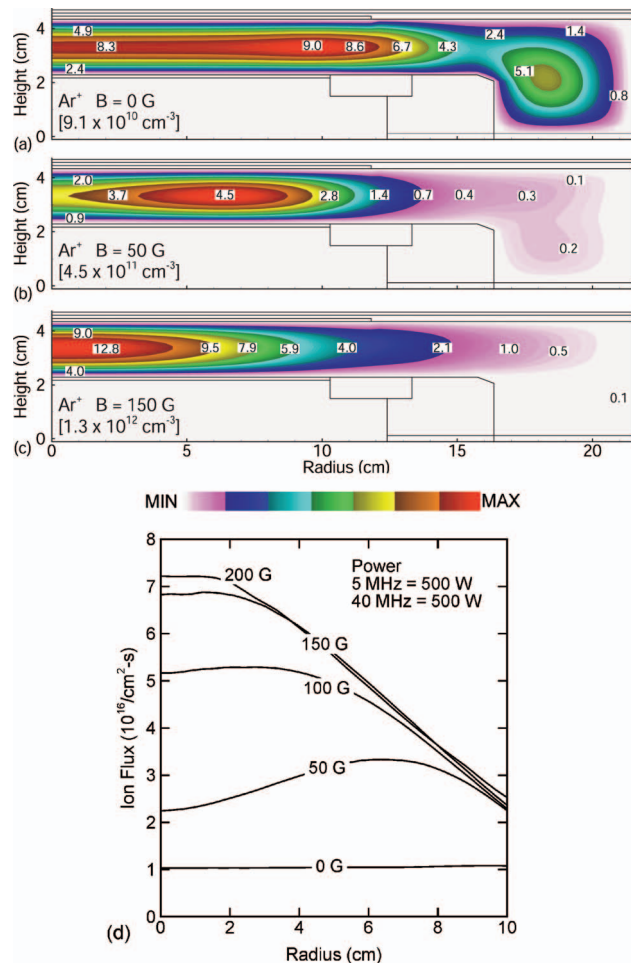


FIG. 3. Time averaged ion densities and fluxes as a function of magnetic field. Ion densities for magnetic fields of (a) 0, (b) 50, (c) 150 G, and (d) ion fluxes to wafer for different magnetic fields. With increasing magnetic field the peak ion density shifts toward the center of the reactor and a gradual convergence of the ion flux occurs.

between the electrodes, the rate of ionization by bulk electrons largely follows the ion density and has a maximum value of 2×10^{16} $\text{cm}^{-3} \text{s}^{-1}$, as shown in Fig. 2. With the sheath 1–2 mm thick, and the mean free path for electron collisions being longer, secondary electrons are launched into the bulk plasma from both electrodes with essentially the instantaneous sheath potential. The LF sheath potential has a maximum value of approximately $V_{LF}+V_{HF}-V_{dc}$ or 343 V. The mean free path for electrons in argon at 40 mTorr at this energy is 4 cm, in excess of the interelectrode spacing of 2 cm. As a result, the secondary electrons largely pass through the plasma producing little ionization (maximum value 1×10^{15} $\text{cm}^{-3} \text{s}^{-1}$).

T_e , S_b , and S_{eb} are shown in Fig. 4 for $B=150$ G for LF =5 MHz (500 W, 202 V, $V_{dc}=-1$ V) and HF=40 MHz (500 W, 140 V). As with the $B=0$ case, to deposit the same power, the voltage on the HF electrode is lower than that on the LF electrode. The Larmor radius for 4 eV electrons with this magnetic field is 0.03 cm. As such, the cross field mobility of ions exceeds that for the electrons. Sheath heating at both electrodes is largely local due to the inability of elec-

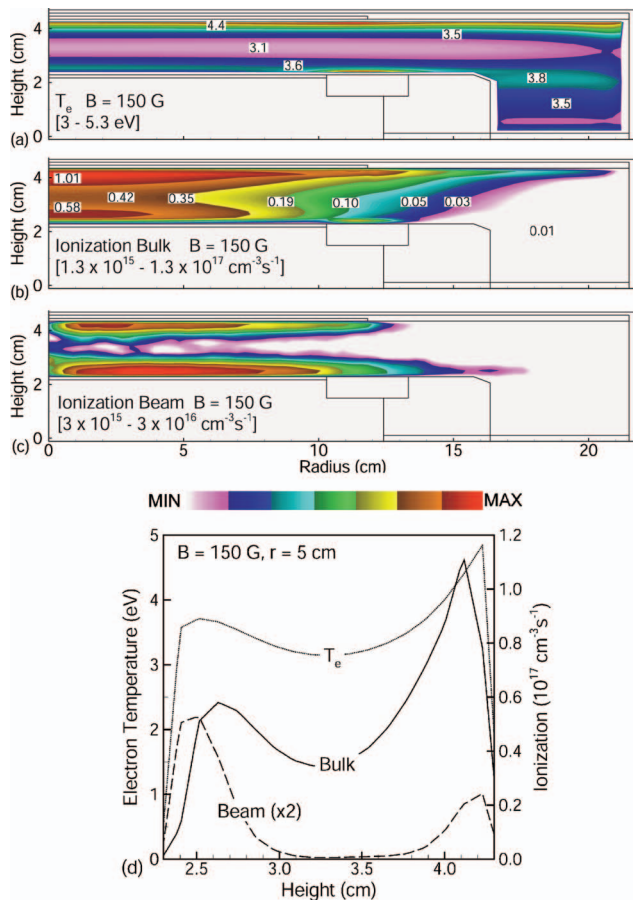


FIG. 4. Plasma properties for $B=150$ G for the base case (Ar, 40 mTorr, $P_{LF}=P_{HF}=500$ W, $\nu_{LF}=5$ MHz, $\nu_{HF}=40$ MHz). (a) Electron temperature, (b) ionization by bulk electrons, (c) ionization by beam electrons, and (d) axial values of these quantities at a radius of 5 cm. The maximum value or range of values in each frame is noted. The bulk and beam ionization have log scales over 2 decades. Contour labels for bulk ionization have units of 10^{17} $\text{cm}^{-3} \text{s}^{-1}$. The bulk and beam ionization sources are confined to be closer to the electrodes by the high magnetic field.

trons to rapidly convect into the bulk plasma. As a result, there are peaks in T_e at both electrodes and a local minimum in T_e in the bulk plasma. The maximum value of T_e , 5.2 eV, exceeds that without the magnetic field due to the more local power deposition. The parallel component of electron mobility along the magnetic field lines enables convection of electron energy into the periphery of the reactor. This creates a disk of high T_e above both electrodes. In spite of the lower voltage at the HF electrode, the peak in T_e there exceeds that at the LF electrode due to the more efficient electron heating at the higher frequency. Secondary electrons are more efficiently used as an ionization source with the magnetic field due to their being trapped on the magnetic field lines and depositing their power in the plasma. As a result, there are peaks in S_{eb} at both electrodes. Opposite to ionization by the bulk electrons, S_{eb} has a higher peak value near the LF electrode. This is a consequence of its larger sheath voltage which launches higher energy secondary electrons into the plasma.

The peak ion density increases by a factor of 13 to 1.3×10^{12} cm^{-3} with $B=150$ G compared to the case without a magnetic field. The distribution of ion density is more center peaked compared to the distribution without a magnetic field. This increase results, in part, from a better utilization of secondary electrons for ionization and a decrease in diffusion losses to the upper and lower electrodes due to the decrease in the transverse value of μ_e . There is a gradual convergence of the ion flux to the wafer from being nearly uniform with $B=0$ to being center peaked with $B=200$ G, as shown in Fig. 3. This trend is not necessarily a characteristic of two-frequency MERIEs in general but is likely a consequence of the decrease in the cross field mobility of electrons, μ_e , compared to ions, μ_i , and charging of dielectrics in this particular geometry, as discussed later. Note that in spite of a large increase in the plasma density and higher utilization of secondary electrons for ionization, the voltage required to deposit 500 W by both sources increases relative to the $B=0$ case. This increase is due to the decrease in the cross field mobility of charge carriers. The increase in voltage is required to increase the bulk electric field to drive the current across the magnetic field lines.

B. Influence of charging of dielectrics

In an electropositive plasma, $\mu_e > \mu_i$, the transient loss of electrons prior to the establishment of ambipolar fields during the creation of the plasma produces a net positive charge in the plasma. This net charge then creates the outwardly pointing ambipolar field that accelerates ions out of the plasma, while slowing the rate of electron loss, so that electron and ion losses are equal. If the walls of the discharge are dielectric, the missing electrons reside on the walls as surface charge. In a MERIE discharge in the transverse direction $\mu_e < \mu_i$, and so the loss of positive charge to surfaces is more likely than the loss of negative charge. As a result, at times during the rf cycle, dielectrics may charge positively (instead of negatively) to slow the loss of the more mobile positive charge. These positively charged surfaces then affect the uniformity of the plasma.

These trends are illustrated by the electric potential at different times during the rf cycle appearing in Figs. 5 and 6 for $B=0$ and $B=200$ G. The frequencies are LF=5 MHz and HF=40 MHz. For $B=0$, the electric potential has the characteristic shape of an electropositive plasma. The potential of the bulk plasma generally sits above the potential of any surface in contact with the plasma. As both the LF and HF electrodes oscillate during their respective cycles the bulk plasma potential also oscillates in such a manner to be at a higher value than either electrode. With a magnetic field, there are significant voltage drops across the bulk plasma, as will be discussed later.

Take note of the electric potential on the surface of focus ring 1 and on the dielectric surrounding the HF electrode with and without a magnetic field. These dielectrics are functionally capacitors which charge and discharge with a RC time constant determined by their own physical capacitances and the resistance of current flow through the plasma to their

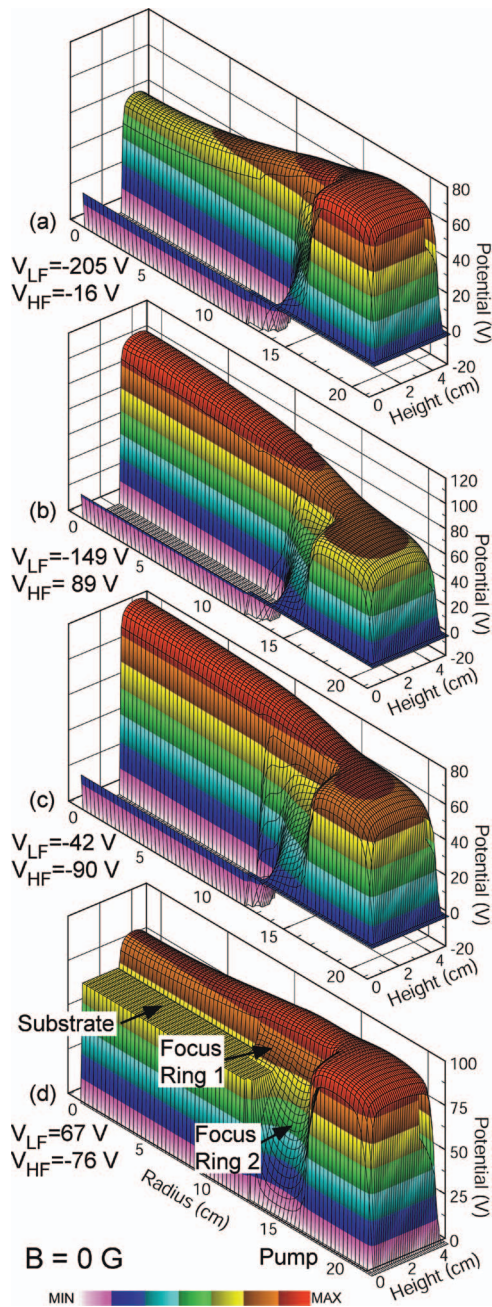


FIG. 5. Electric potential for $B=0$ at different times during the rf cycle. The conditions are otherwise the same as the base case (Ar, 40 mTorr, $P_{LF}=P_{HF}=500$ W, $\nu_{LF}=5$ MHz, $\nu_{HF}=40$ MHz). The potential on the surface of focus ring 1 is essentially always at the local plasma potential due to the large μ_e .

surfaces. With $B=0$, μ_e is large enough that the RC time constants are smaller than the rf period at either the LF or HF. As a result, the surface of, for example, the focus ring is essentially always at the local plasma potential (or displaced negative to the local plasma potential by the floating sheath potential). A voltage drop occurs through the focus ring from its surface potential to the biased substrate below it.

With $B=200$ G, μ_e is smaller than μ_i . Both mobilities are small enough that the plasma resistance increases to such a large value that the RC time constant of the dielectrics ex-

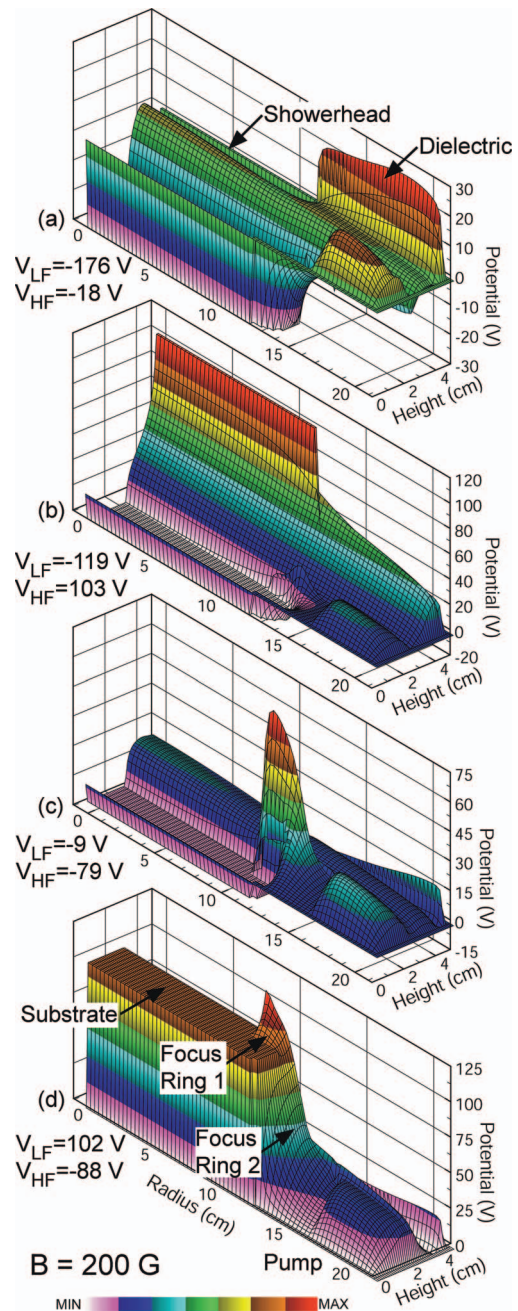


FIG. 6. Electric potential for $B=200$ G at different times during the rf cycle. The conditions are otherwise the same as the base case (Ar, 40 mTorr, $P_{LF}=P_{HF}=500$ W, $\nu_{LF}=5$ MHz, $\nu_{HF}=40$ MHz). The positive charge collected by the dielectric surface surrounding the wafer during the LF and HF cathodic cycles charges those surfaces positive and is neutralized by electrons during the LF and HF anodic cycles.

ceeds the HF period and is commensurate to the LF period. Additionally, with $\mu_e < \mu_i$, the plasma acts as though it is electronegative. That is, the positive charge, being more mobile, more rapidly escapes from the plasma. Under these conditions, surfaces will naturally charge positively. As a result, during the cathodic part of the cycle of both the HF and LF electrodes when ions are accelerated into the surrounding dielectrics, the dielectrics charge positively to slow the flux of additional ions to their surfaces. The excess positive

charge produces a positive potential on the top dielectric as shown in Fig. 6(a) and on focus ring 1 as shown in Fig. 6(c). As the voltage on the electrodes begins to increase toward more positive values and enters the anodic part of the cycle, electron flux is attracted to the dielectric surfaces and the excess positive charge is dissipated. This neutralization of the positive charge (and reduction in surface potential of the dielectrics) is shown in Fig. 6(b) for the HF electrode and Fig. 6(d) for the LF electrode.

As the B field increases, the length of time into the anodic part of the cycle which the dielectric surfaces remain charged positively increases. It is this peripheral positive charge with increasing B field that contributes to the convergence of the ion flux towards the center of the wafer shown in Fig. 3.

C. Secondary electron emission coefficients

It is well known that the secondary electron emission coefficient, γ , is a function of both energy of the ion and the condition of the electrodes.²¹ γ may increase (or decrease) by an order of magnitude or more depending on the condition of the electron emitting surface. MERIE plasma tools may be particularly sensitive to variations in γ resulting from the conditioning of surfaces due to their higher utilization of secondary electrons as a source of ionization. This sensitivity is illustrated by the following computer experiment.

A single frequency MERIE is operated with 100 mTorr argon with a constant voltage for $B=0$ G ($V=170$ V) and for $B=100$ G ($V=200$ V) while varying γ from 0.01 to 0.45. The resulting ion density and power deposition are shown in Fig. 7. For $B=0$, over this range of γ the ion density increases by only 5% from 1.3×10^{10} cm⁻³ for the smallest value of γ . The power dissipation actually decreases by about 10%. Due to the long mean free path of the secondary electrons, the majority of the electrons pass through the plasma producing little additional ionization while not dissipating their power. As a result, the plasma appears more capacitive and so the power dissipation decreases.

With $B=150$ G, the vast majority of the secondary electron energy is converted to excitation and ionization since the Larmor radius is small enough to confine the secondary electrons to the gap. With a constant voltage, an increase in γ and ionization produces a commensurate increase in ion density (increasing by a factor of 4 from 1.5×10^{10} cm⁻³) and power deposition (increasing by a factor of 3).

D. Electric potentials and sheath voltages

With the applied voltage oscillating at both the LF and HF, the plasma potential has both frequency components, as shown in Fig. 8(a) for $B=0$ and in Fig. 9(a) for $B=150$ G. The plasma potential has excursions to its maximum value at the peak of the anodic part of the LF cycle, reflecting both the higher value of the LF voltage ($V_{LF}=193$ V with $V_{dc}=-22$ V, $V_{HF}=128$ V) and contributions from the HF. In the absence of the HF the plasma potential would be pegged at near its floating potential when the LF cycle is in its cathodic phase. With the HF, the plasma potential oscillates

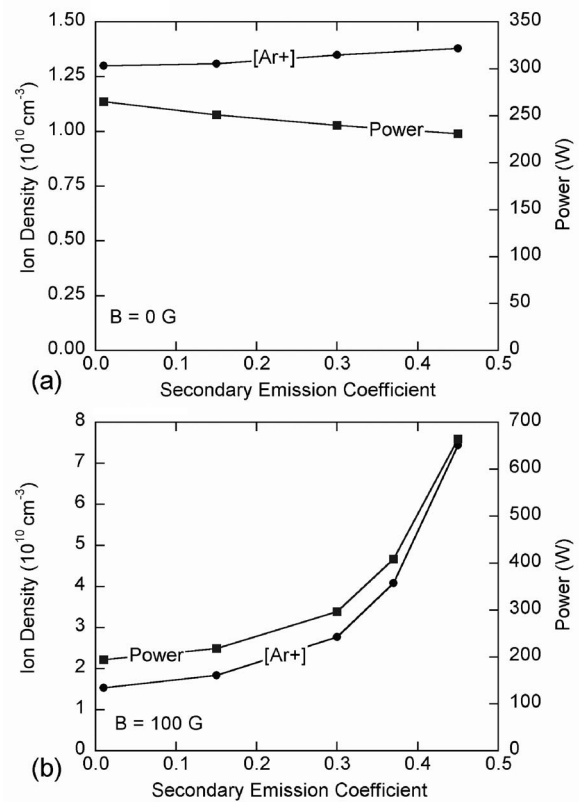


FIG. 7. Argon ion density and power deposition as a function of secondary electron emission coefficient for different magnetic fields with constant voltage. (a) $B=0$ ($V=170$ V) and (b) $B=150$ G ($V=200$ V). The increase in the argon ion density with increasing γ is greater with the magnetic field as a result of more efficient utilization of beam electrons for ionization.

commensurate with the oscillation with the HF voltage in order to keep its value positive with respect to all surfaces, including the HF electrode. The plasma potential for the $B=150$ G case [Fig. 9(a)] has a similar time dependence ($V_{LF}=202$ V with $V_{dc}=-1$ V, $V_{HF}=140$ V), however, its shape indicates a more resistive plasma commensurate with the decrease in cross field mobilities.

The spatial distributions of electric potential through the bulk plasma differ markedly for the $B=0$ and $B=150$ G cases. For example, the plasma potential at $r=5$ cm is shown in Fig. 8(b) for $B=0$ for approximately the peak of the LF anodic cycle (phase $\phi=\pi/2$), peak of LF cathodic cycle ($\phi=3\pi/2$), and the zero crossing in the LF rf voltage ($\phi=0$) displaced by V_{dc} . These values are shown when $V_{HF}=0$. The corresponding values are shown in Fig. 8(c) for the HF cycle when V_{LF} is approximately zero. At all phases, at both the LF and HF electrodes, the sheaths are electropositive. That is, the sheaths are electron repelling and ion attracting. The bulk plasma is electropositive, as indicated by the small positive potential in the center of the plasma through nearly all phases. This indicates that the diffusive electron flux to the electrodes, modulated by the sheath potential, carries the majority of the rf current.

Plasma potentials for the same phases are shown in Figs. 9(b) and 9(c) for $B=150$ G. Due to the low values of μ_e and

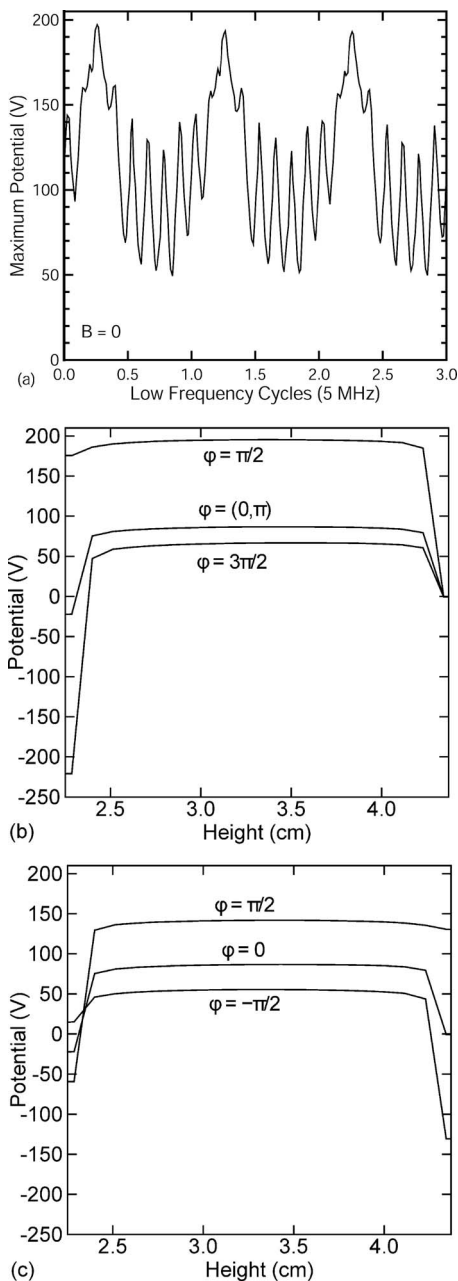


FIG. 8. Plasma potential for the base case (Ar, 40 mTorr, $P_{LF}=P_{HF}=500$ W, $\nu_{LF}=5$ MHz, $\nu_{HF}=40$ MHz) with $B=0$. (a) Maximum plasma potential as a function of LF cycles, (b) plasma potential as a function of height at radius $r=5$ cm at different fractional phases during the LF cycle, and (c) plasma potential as a function of height at different fractional phases during the HF cycle. The HF and LF sheaths are electropositive through the entire rf cycles.

μ_i , the bulk plasma is resistive. To drive current through the plasma, a large electric field is required, approximately 30 V/cm. The voltage that is dropped across the bulk plasma to drive the current is not available to be dropped across the sheath and so is not available for ion acceleration. During the LF cycle, ion current is collected during the cathodic part of the cycle during which the sheaths appear electropositive. During the anodic part of the LF cycle electron current should be collected. μ_e is so small that the sheath must re-

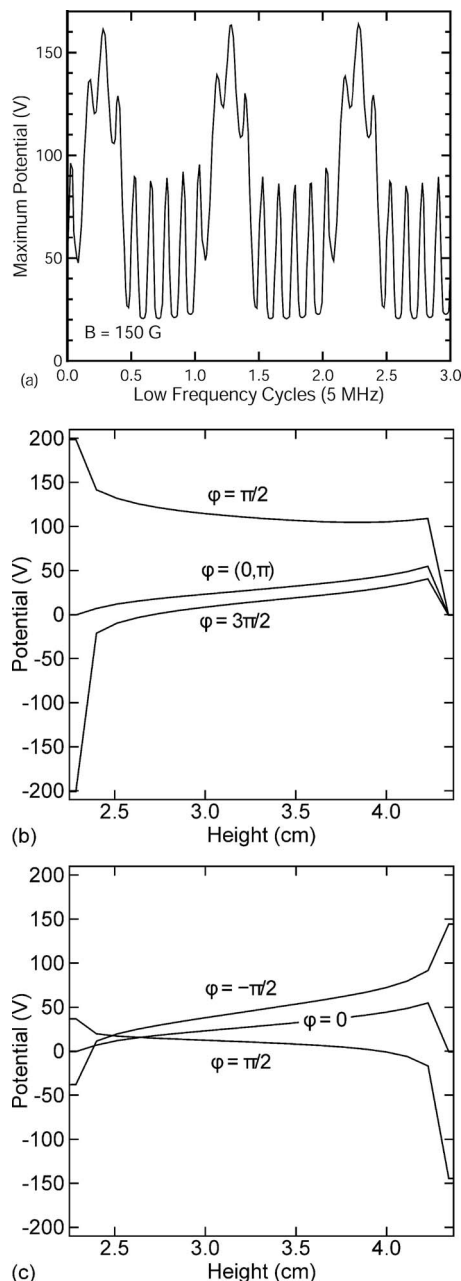


FIG. 9. Plasma potential for the base case (Ar, 40 mTorr, $P_{LF}=P_{HF}=500$ W, $\nu_{LF}=5$ MHz, $\nu_{HF}=40$ MHz) with $B=150$ G. (a) Maximum plasma potential as a function of LF cycles, (b) plasma potential as a function of height at radius $r=5$ cm at different fractional phases during the LF cycle, and (c) plasma potential as a function of height at different fractional phases during the HF cycle. Sheath reversals occur at both the LF and HF electrodes.

verse (that is, become electron attracting and ion repelling) to collect enough electron current. This reversal in the direction of the electric field penetrates more than a centimeter into the plasma.

A similar phenomenon occurs at the HF electrode. During the cathodic part of the HF cycle, the sheath appears electropositive. During the anodic part of the cycle, insufficient electron current is collected and so the electric field in the sheath must reverse to become ion repelling and electron

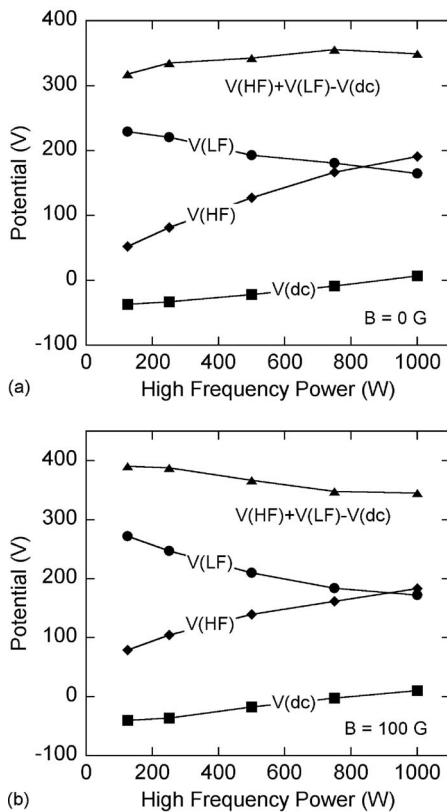


FIG. 10. Electrical parameters V_{LF} , V_{HF} , V_{dc} and their sum, E_m , as a function of HF power. (a) $B=0$ and (b) $B=100$ G. V_{HF} increases to deliver a larger P_{HF} and V_{LF} decreases with increasing P_{HF} to maintain P_{LF} constant. The goal of keeping E_m a constant is nearly met but only fortuitously.

attracting. The reversal of the electric field in the bulk plasma begins before the zero crossing in V_{HF} and extends across the entire plasma for the majority of the anodic half of the cycle. Again, the voltage drop across the bulk plasma that is required to drive electron current to the high voltage sheath is that much less voltage available for ion acceleration across the sheath.

The reversals of the electric fields in the sheaths and the increasingly resistance of the bulk plasma with increasing B field have important implications with respect to the ion energy and angular distributions (IEADs) that are incident onto the wafer. Neglecting floating potentials and assuming negligible voltage drop across the bulk plasma, the maximum ion energy onto the wafer is $E_m = V_{\text{LF}} + V_{\text{HF}} - V_{\text{dc}}$. This condition corresponds to when the LF electrode is at the minimum voltage of the cathodic cycle (offset by any additional dc bias) thereby dropping its entire voltage across the sheath; and the HF electrode is at the maximum voltage of its anodic cycle, thereby raising the potential of the bulk plasma by an additional V_{HF} .

In our investigation, we have specified power and adjusted the voltages on the LF and HF electrodes to deliver that power. For example, V_{LF} , V_{HF} , and V_{dc} are shown in Fig. 10 for keeping $P_{\text{LF}} = 500$ W and varying P_{HF} from 100 to 1000 W. Results are shown for $B=0$ and $B=100$ G. With $B=0$, in order to deliver a larger power, V_{HF} increases nearly

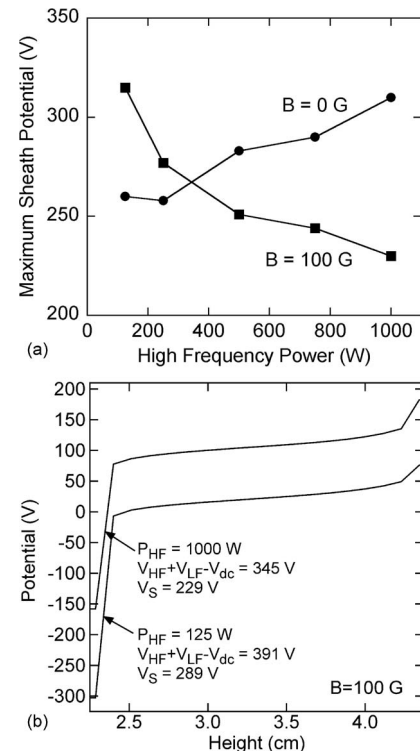


FIG. 11. Potentials for different HF powers. (a) The maximum LF sheath potential as a function of HF power with $B=0$ and $B=100$ G and (b) the plasma potential as a function of height for $B=100$ G at $r=5$ cm for $P_{\text{HF}} = 125$ W and 1000 W.

linearly with P_{HF} . As the plasma density increases with increasing P_{HF} , a larger potential current source is produced for the LF electrode. To deliver the same power, V_{LF} can then decrease. The decrease in V_{LF} is also nearly linear with P_{HF} . For these conditions and geometry, the plasma becomes more symmetric with increasing P_{HF} and so V_{dc} decreases (becomes less negative). The end result is that E_m increases from 310 V for $P_{\text{HF}}=100$ W to 350 V for $P_{\text{HF}}=1000$ W. Although the goal of maintaining E_m a constant so that IEADs are unchanged when varying P_{HF} is nearly met, this goal is only fortuitously met. The constant value of E_m results from commensurate decreases in V_{LF} as V_{HF} increases.

Similar trends are obtained for $B=100$ G. As P_{HF} increases, V_{HF} increases while V_{LF} decreases. Here, however, the decrease in V_{LF} is proportionately larger than the increase in V_{HF} . As a result, E_m decreases from 390 to 345 V, opposite the trend with $B=0$. Again, the goal of maintaining E_m a constant is nearly met but only fortuitously.

Unfortunately, the maintenance of a constant E_m with $B=100$ G does not translate into maintaining uniform IEADs. This trend is due to the large voltage drop across the bulk plasma resulting from the increase in plasma resistance. For example, the maximum sheath potential at the LF electrode, V_S , obtained with the model is shown in Fig. 11(a) as a function of P_{HF} for $B=0$ and $B=100$ G. When $B=0$, V_S increases with increasing P_{HF} in spite of V_{LF} decreasing. This increase in V_S results from the increase in V_{HF} , whose amplitude raises the plasma potential at the peak of its anodic

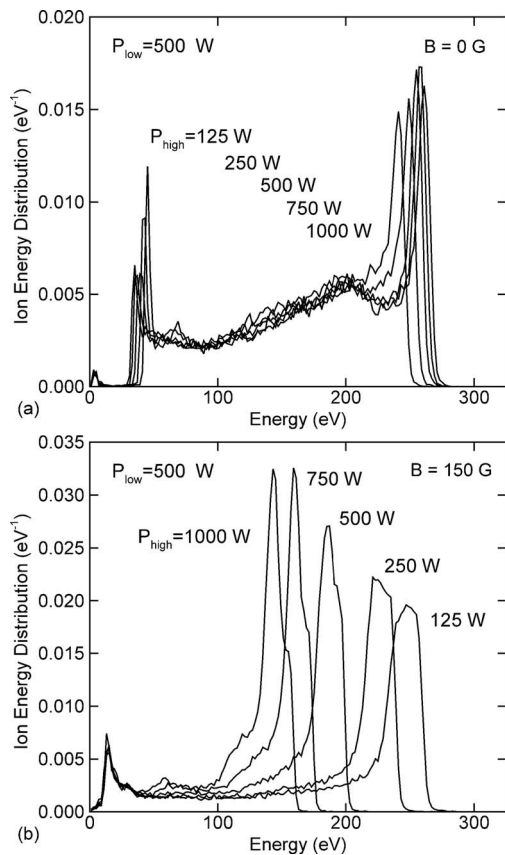


FIG. 12. Ion energy distributions incident on the wafer (integrated over angle) while varying the high frequency power for (a) $B=0$ and (b) $B=150$ G. At $B=150$ G, the voltage drop across the bulk plasma and the reversal of the HF sheath causes the successive shift of the peak of the IED to lower energy.

cycle, which adds to V_{LF} at the minimum of its cathodic cycle. For $B=100$ G, V_S decreases with increasing P_{HF} in spite of an increase in V_{HF} . The reason is that the sheath reversal at the HF electrode and the voltage drop across the bulk plasma remove HF voltage that would otherwise add to V_S at the LF electrode.

Plasma potentials as a function of height for $B=100$ G at $r=5$ cm for $P_{HF}=125$ W and 1000 W are shown in Fig. 11(b). These profiles are for when the LF electrode is at the minimum of the cathodic part of the cycle and the HF electrode is at the maximum of the anodic part of the cycle. These are conditions for which V_S should have its maximum value of E_m . For $P_{HF}=125$ W, the maximum value of $E_m=391$ V whereas the actual value of $V_S=289$ V. The difference of 102 V is dropped roughly half across the bulk plasma and half across the sheath reversal at the HF electrode. Similarly for $P_{HF}=1000$ W, the maximum value of $E_m=345$ V whereas the actual value of $V_S=229$ V. The difference of 116 V is dropped across the bulk plasma and the reversed sheath at the HF electrode.

E. Ion energy distributions: Power applied to one and two electrodes

These disparities in the scaling of V_S with and without a magnetic field when varying P_{HF} produce similar disparities

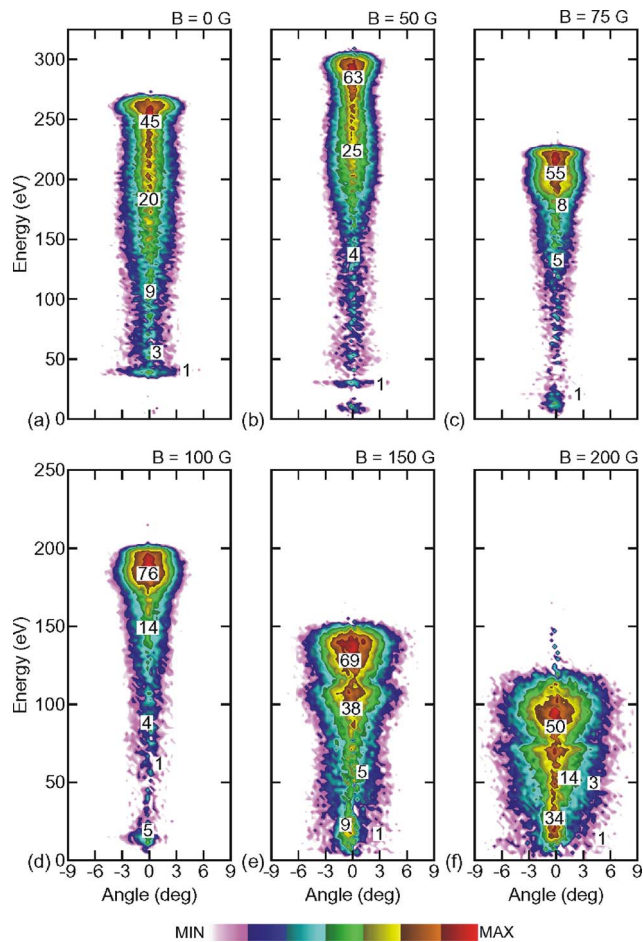


FIG. 13. IAEDs striking the substrate for the base case (Ar, 40 mTorr, $P_{LF}=P_{HF}=500$ W, $\nu_{LF}=5$ MHz, $\nu_{HF}=40$ MHz) while varying magnetic field from 0 to 200 G. The IAEDs have units of $\text{eV}^{-1} \text{sr}^{-1}$. The contours span 2 decades using a log scale. Labels are percentages of the maximum value. For moderate and high magnetic fields, the decrease in V_S with increasing magnetic field and the sheath reversal during the anodic part of the rf cycle result in the downshift in energy and spread in angle of IAEDs.

in the scaling of ion energy distributions (IEDs). The angularly integrated IEDs incident on the wafer for $B=0$ and $B=150$ G are shown in Fig. 12 while varying P_{HF} from 125 to 1000 W. P_{LF} is held constant at 500 W. With $B=0$, as P_{HF} increases the shapes of the IEDs stay nearly constant with about a 10% increase in the energy of the peak of the IED. These trends mirror the nearly constant (but slightly increasing) value of E_m . On the other hand, with $B=150$ G the energy of the peak of the IED decreases from 250 to 125 eV as P_{HF} increases from 125 to 1000 W. The aforementioned voltage drop across the bulk plasma and reversal of the anodic sheath which removes voltage from V_S are responsible. The fact that the sheath at the HF electrode is reversed at the anodic maximum of the HF cycle means that the increase in V_{HF} with increasing P_{HF} does not fully contribute to increasing V_S . The peak of the IED then decreases because V_{LF} decreases.

IAEDs as a function of magnetic field are shown in Fig. 13 for $P_{LF}=P_{HF}=500$ W. With the exception of the applications of small magnetic fields (<50 G), the IAEDs generally

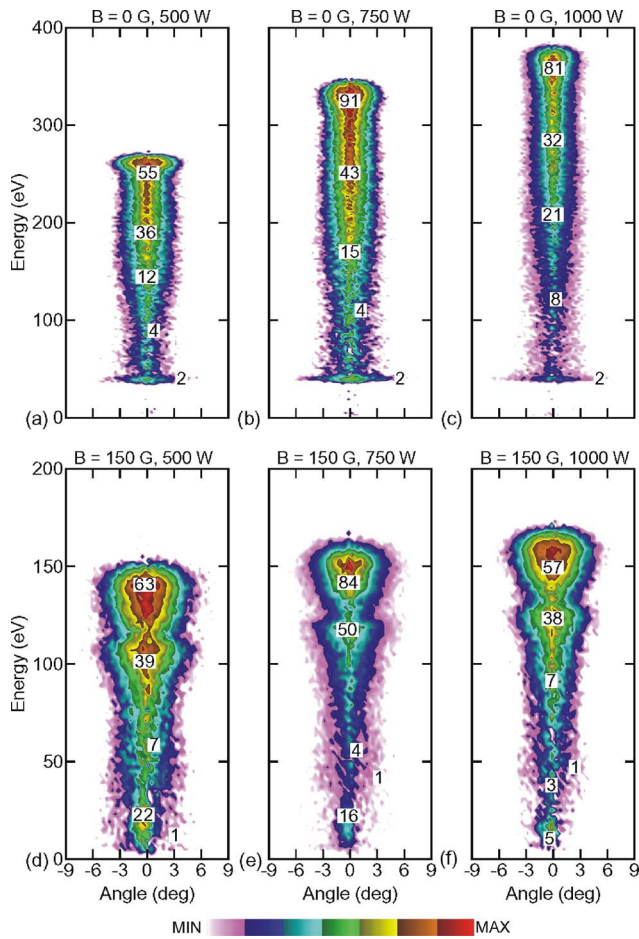


FIG. 14. IEDs striking the substrate for the base case for $P_{HF}=500$ W while varying P_{LF} from 500 to 1000 W. (a)–(c) $B=0$ and (d)–(f) $B=150$ G. The IEDs have units of $\text{eV}^{-1} \text{sr}^{-1}$. The contours span 2 decades using a log scale. Labels are percentages of the maximum value. When P_{LF} increases above P_{HF} , the plasma density increases and the LF voltage does not increase linearly with power.

shift to lower energies and broaden in angle with increasing B field. These trends are caused by the decrease in V_S with increasing B field resulting from voltage being dropped across the bulk plasma and the deceleration ions experience during the anodic part of the rf cycle when the LF sheath reverses. These trends are similar to those seen with single frequency MERIEs.^{16,17}

IEDs for $P_{LF}=500, 750,$ and 1000 W with and without a magnetic field are shown in Fig. 14. P_{HF} is held constant at 500 W. The expectation is that the peak energy and shape of the IEDs should be controlled by P_{LF} in a fairly linear fashion. In principle, holding P_{HF} constant fixes the ion current and increasing P_{LF} should only extend the IED to higher energies while keeping the angular spread nearly constant. This is, in fact, what is observed with $B=0$, however, not in a strictly linear fashion. As P_{LF} exceeds P_{HF} , increasing P_{LF} also increases the plasma density thereby increasing the efficiency of power deposition. As a result, only a 50% increase in V_{LF} (from 193 to 289 V) is required to double the LF power deposition. With the limited increases in V_{LF} and a

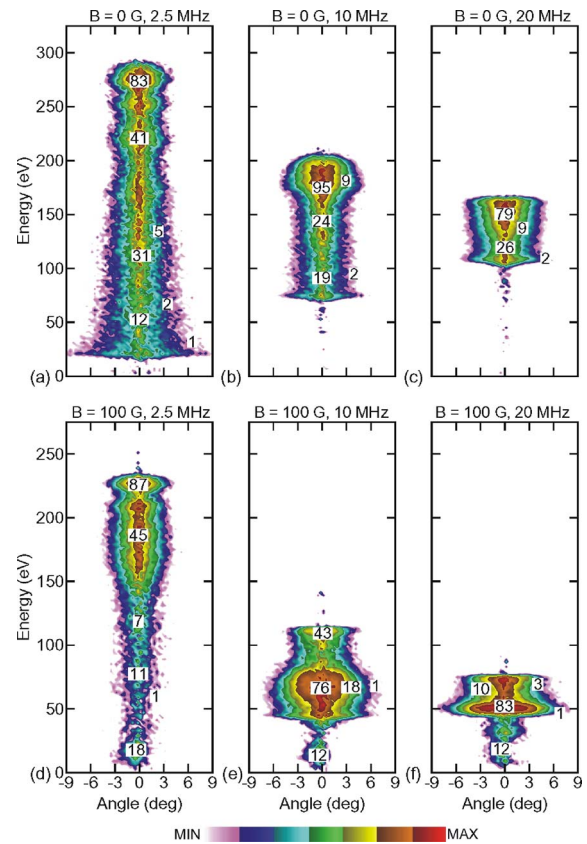


FIG. 15. IEDs incident onto the substrate for ν_{LF} of 2.5, 10, 20 MHz with (a)–(c) $B=0$ and (d)–(f) $B=100$ G. The IEDs have units of $\text{eV}^{-1} \text{sr}^{-1}$. The contours span 2 decades using a log scale. Labels are percentages of the maximum value. The IEDs narrow in energy as ν_{LF} increases. For $B=100$ G, the reversal of the sheath during the anodic part of the rf cycle result in the persistence of low energy peaks in IEDs.

small decrease in the amplitude of V_{HF} due to the higher plasma density, the maximum energy of the IEDs does not double with a doubling of P_{LF} .

For low values of P_{LF} with $B=150$ G, the sheath is reversed during a significant fraction of the rf cycle. This results in an angularly broad IED extending to nearly zero energy. Upon increasing P_{LF} , a smaller fraction of the rf cycle has a sheath reversal, and so the IEDs not only increase their extent in energy, but also narrow in angle. However, the extension in the energy of the IEDs with increasing P_{LF} is less compared to that for $B=0$. This difference can be attributed to at least two effects: the more efficient utilization of secondary electrons and the dependence of dc bias on magnetic field.

At $B=150$ G, the secondary electrons are well confined by the magnetic field thereby providing additional ionization sources. This more efficient utilization of secondary electrons facilitates more efficient power deposition and reduces the increase in V_{LF} required to double P_{LF} (from 201 to 235 V). A second contributing cause to there being less extension of the IEDs is the behavior of the dc bias. With $B=0$, the dc bias becomes more negative with increasing P_{LF} , thereby contributing to an increase in ion energy. However, at $B=150$ G, the proportions of the current being carried by ions

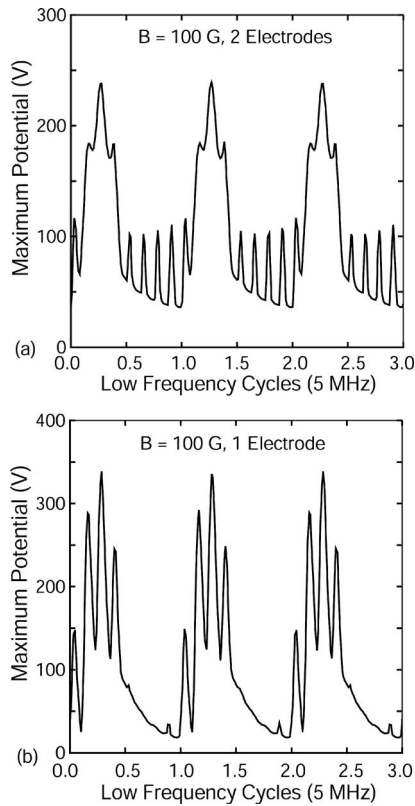


FIG. 16. Maximum plasma potential during three LF rf cycles for constant applied voltage ($V_{LF}=250$ V, $V_{HF}=150$ V) with $B=100$ G. (a) The LF and HF sources applied to separate electrodes and (b) both sources are applied to the same electrode. The conditions are otherwise the same as the base case (Ar, 40 mTorr, $\nu_{LF}=5$ MHz, $\nu_{HF}=40$ MHz). By switching to the same electrode the large negative V_{LF} nearly eliminates the contribution of the V_{HF} to the plasma potential during the LF cathodic cycle.

and electrons are about same and the dc bias is nearly unaffected by the change in plasma density. V_{dc} therefore does not contribute to extending the IEADs with increasing P_{LF} as with $B=0$.

Another method of controlling the IEAD is to adjust the frequency of the rf source. As is well known, IEADs generally narrow in energy as the frequency increases due to the finite time required for ions to cross the sheath. For example, IEADs while varying the LF frequency, ν_{LF} , are shown in Fig. 15 for $B=0$ and 100 G while keeping P_{LF} constant. With $B=0$ and with P_{LF} constant, V_{LF} decreases with increasing ν_{LF} to reflect the more efficient electron heating at higher ν_{LF} . Correspondingly, V_{HF} increases to compensate for the decreasing stochastic heating at the HF sheath due to the decrease in V_{LF} . The end result is that E_m remains nearly unchanged. The final outcome is the IEADs narrow in energy as ν_{LF} increases while the angular spread remains nearly constant. With $B=100$ and with P_{LF} constant, the decrease in V_{LF} with increasing ν_{LF} is proportionately larger in part because the plasma density is larger. Thus E_m decreases and the IEADs undergo more degradation in energy and more angular spreading than without a magnetic field. The low energy tails of the IEADs persist at high ν_{LF} due to the sheath reversal during the anodic phase of the LF cycle.

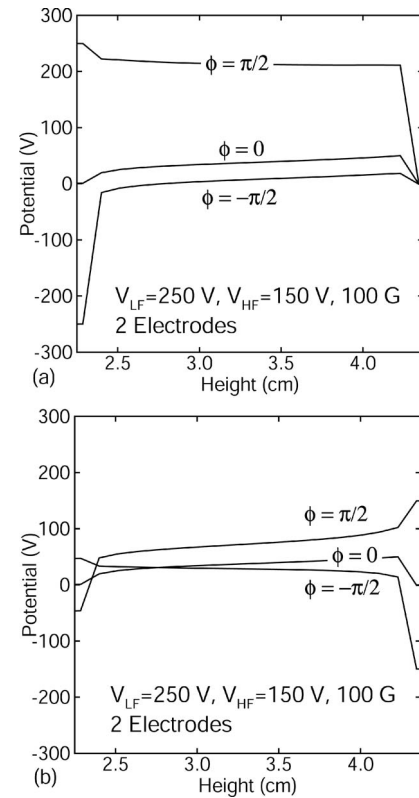


FIG. 17. Plasma potential when the HF and LF sources are applied to separate electrodes at different times during the rf cycle for constant applied voltage ($V_{LF}=250$ V, $V_{HF}=150$ V) with $B=100$ G. (a) Plasma potential as a function of height at radius $r=5$ cm at different fractional phases during the LF cycle and (b) for different fractional phases during the HF cycle.

The HF and LF powers can be applied to the same electrode and we compared such sources to the two powered electrode variant discussed thus far. In comparing these two sources, we kept the amplitudes of the applied voltages constant at $V_{HF}=150$ V and $V_{LF}=250$ V and forced V_{dc} to be zero. The intent was to isolate changes in plasma properties resulting from only where the LF and HF powers were applied.

The maximum plasma potential is shown in Fig. 16 as a function of LF cycles for the two- and one-electrode sources with $B=100$ G. With the applied voltage oscillating at both the LF and HF, the plasma potential has excursions to its maximum value at the simultaneous peaks of the anodic part of the LF and HF cycles. In principle, the plasma potential should have a peak value of nearly $V_{LF}+V_{LF}$ or 400 V. In the two-electrode case, the sheath reversal at the HF electrode and HF voltage drop across the bulk plasma removes voltage that might otherwise raise the plasma potential. As a result, the peak value of the plasma potential is only 240 V.

By also applying the HF source to the lower electrode, the contributions of the HF component to the plasma potential are fundamentally different. During the LF cathodic cycle, the HF components of the plasma potential nearly disappear. This can be attributed to V_{HF} being less than V_{LF} , and so their sum is still negative during most time of the LF cathodic cycle. This eliminates the HF modulation of the plasma po-

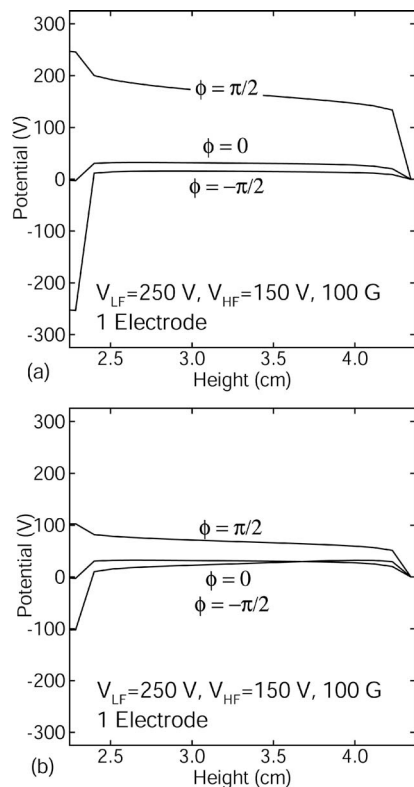


FIG. 18. Plasma potential when the HF and LF sources are applied to the lower electrode at different times during the rf cycle for constant applied voltage ($V_{LF}=250$ V, $V_{HF}=150$ V) with $B=100$ G. (a) Plasma potential as a function of height at radius $r=5$ cm at different fractional phases during the LF cycle and (b) for different fractional phases during the HF cycle.

tential during that part of the LF cycle. On the other hand, with HF and LF on the same electrode, HF voltage directly contributes to raising the plasma potential during the anodic peak of the LF cycle without loss of voltage across the bulk plasma. As a result, the peak plasma potential is 340 V, higher than when voltage is applied to both electrodes.

The plasma potential as a function of height at $r=5$ cm is shown in Fig. 17(a) for the two-electrode case with $B=100$ G for the peak of the LF anodic cycle (phase $\phi = \pi/2$), peak of LF cathodic cycle ($\phi = \pi/2$), and the LF zero crossing voltage ($\phi=0$). These values are shown with $V_{HF}=0$. The corresponding values are shown in Fig. 17(b) for the HF cycle when V_{LF} is approximately zero. Similar to that shown in Fig. 9, the reversal of the electric field in the sheath occurs during both the HF and LF anodic cycle. The corresponding values are plotted in Fig. 18 for the one-electrode case. Although there are sheath reversals during both the LF and HF cycles, the sheath is always electropositive on the upper, now grounded, electrode.

IEADs are shown in Fig. 19 for $B=0$ and 100 G for the one- and two-electrode cases. In principle, applying the HF source to the LF electrode increases the effective frequency of the LF sheath oscillation. The multiple energy peaks in the one-electrode IEADs reflect this high frequency modulation. The result is that IEADs narrow in energy, particularly for $B=0$. The lack of HF oscillation of the plasma potential dur-

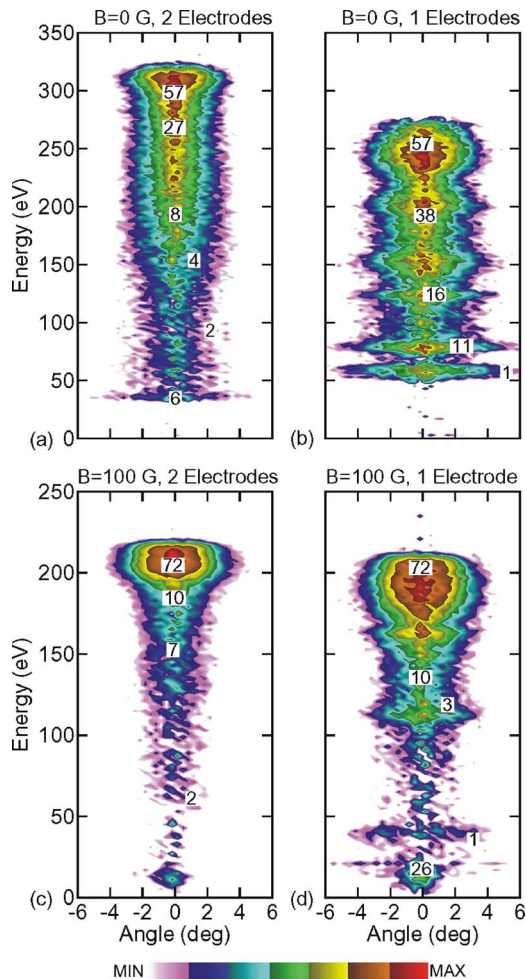


FIG. 19. Comparison of IEADs for applying the HF and LF sources to separate electrodes and the same electrode. (a) Two electrodes and (b) one electrode for $B=0$; and (c) two electrodes and (d) one electrode for $B=100$ G. The IEADs have units of $\text{eV}^{-1} \text{sr}^{-1}$. The contours span 2 decades using a log scale. Labels are percentages of the maximum value. For $B=0$, the narrowing in energy of the IEAD when using the same electrode for both voltages results from the increase of the frequency at which the sheath oscillates. The low energy tail of the IEAD at $B=100$ G persists due to sheath reversal during the LF anodic cycle.

ing the cathodic part of the LF cycle emphasizes and broadens the low energy portion of the IEADs compared to the two-electrode case. With $B=100$ G, similar trends are observed. The IEADs for the one-electrode case have a lower peak energy and more prominent low energy tail.

IV. CONCLUDING REMARKS

The properties of two-frequency MERIE plasma sources sustained in argon have been computationally investigated using results from a two-dimensional plasma transport model. Similar to the single frequency MERIE, two-frequency MERIEs show the trends of localization of plasma density near the powered electrodes and the shift of the peak ion density toward the center of the reactor as the magnetic field increases. The reduction in transverse electron mobility as the magnetic field increases causes a reversal of the electric field in both the HF and LF sheaths and produces an

increase in voltage drop across the bulk plasma. The end result is a decrease in energy and broadening of angle of incidence of ions onto the substrate. The effect described here is likely a worst case as the magnetic field in this model is perfectly parallel to the substrate. In actual plasma reactors there will likely be magnetic field lines that intersect with the face of the substrate which would provide a low impedance path for electrons to the surface. Under such conditions, the magnitude of the sheath reversal would be less.

The convergence of the ion flux toward the center of the wafer with increasing magnetic field can be attributed to the peripheral positive charge collected by the dielectric surfaces during the time the sheaths are reversed at both the LF and HF electrodes. The sheath reversal and the voltage drop across the bulk plasma are responsible for the continuous downward shift in the peak in energy of IEADs as P_{HF} increase while P_{LF} is maintained constant. The plasma potential and IEADs obtained when applying both HF and LF to the same electrode differ from the two-electrode variant. This results in part from the relative amplitudes of the LF and HF components; and the sheath reversal and voltage drop of the HF component across the bulk plasma.

ACKNOWLEDGMENTS

This work was supported by the Semiconductor Research Corp. and the National Science Foundation (Grant No. CTS-0520368).

¹R. A. Lindley, C. H. Bjorkman, H. Shan, K.-H. Ke, K. Doan, R. R. Mett,

- and M. Welch, *J. Vac. Sci. Technol. A* **16**, 1600 (1998).
- ²K. E. Davies, M. Gross, and C. M. Horwitz, *J. Vac. Sci. Technol. A* **11**, 2752 (1993).
- ³M. J. Buie, J. T. P. Pender, and P. L. G. Ventzek, *Jpn. J. Appl. Phys., Part 1* **36**, 4838 (1997).
- ⁴P. Berruyer, F. Vinet, H. Feldis, R. Blanc, M. Lerme, Y. Morand, and T. Poiroux, *J. Vac. Sci. Technol. A* **16**, 1604 (1998).
- ⁵G. A. Hebner, E. V. Barnat, P. A. Miller, A. M. Paterson, and J. P. Holland, *Plasma Sources Sci. Technol.* **15**, 879 (2006).
- ⁶V. Georgieva and A. Bogaerts, *J. Appl. Phys.* **98**, 023308 (2005).
- ⁷T. Kitajima, Y. Takeo, Z. Lj. Petrovic, and T. Makabe, *Appl. Phys. Lett.* **77**, 489 (2000).
- ⁸W. Tsai, G. Mueller, R. Lindquist, B. Frazier, and V. Vahedi, *J. Vac. Sci. Technol. B* **14**, 3276 (1996).
- ⁹P. C. Boyle, A. R. Ellingboe, and M. M. Turner, *J. Phys. D* **37**, 697 (2004).
- ¹⁰P. A. Miller, E. V. Barnat, G. A. Hebner, A. M. Paterson, and J. P. Holland, *Plasma Sources Sci. Technol.* **15**, 889 (2006).
- ¹¹E. V. Barnat, P. A. Miller, G. A. Hebner, A. M. Paterson, T. Panagopoulos, E. Hammond, and J. Holland, *Plasma Sources Sci. Technol.* **16**, 330 (2007).
- ¹²Z. Donko and Z. Lj. Petrovic, *Jpn. J. Appl. Phys., Part 1* **45**, 8151 (2006).
- ¹³L. Z. Tong and K. Nanbu, *Europhys. Lett.* **75**, 63 (2006).
- ¹⁴H. H. Goto, H. Lowe, and T. Ohmi, *J. Vac. Sci. Technol. A* **10**, 3048 (1992).
- ¹⁵S. Rauf, *IEEE Trans. Plasma Sci.* **31**, 471 (2003).
- ¹⁶M. J. Kushner, *J. Appl. Phys.* **94**, 1436 (2003).
- ¹⁷A. V. Vasenkov and M. J. Kushner, *J. Appl. Phys.* **95**, 834 (2004).
- ¹⁸A. Perret, P. Chabert, J. P. Booth, J. Jolly, J. Guillon, and Ph. Auvray, *Appl. Phys. Lett.* **83**, 243 (2003).
- ¹⁹M. A. Lieberman, J. P. Booth, P. Chabert, J. M. Rax, and M. M. Turner, *Plasma Sources Sci. Technol.* **11**, 283 (2002).
- ²⁰P. Subramonium and M. J. Kushner, *J. Vac. Sci. Technol. A* **20**, 313 (2002).
- ²¹A. V. Phelps and Z. Lj. Petrović, *Plasma Sources Sci. Technol.* **8**, R21 (1999).